A web-based histology atlas for the freshwater crustacean *Daphnia magna*

Short title: Web-based *Daphnia* histology atlas

Mee S. Ngu[1,2], Daniel J. Vanselow[1,2], Carolyn R. Zaino[1,2], Debra A. Shearer[2], Chadwick Harris[1], Maksim A. Yakovlev[1,2], Spencer R. Katz[1,2], Alex Y. Lin[1,2], Jean E. Copper[1,2], Dula Parkinson[3], Margaret J. Beaton[4], John K. Colbourne[5], Keith C. Cheng[1,2,*], Khai C. Ang[1,2,*]

[1]Department of Pathology, Pennsylvania State University College of Medicine, Pennsylvania, USA

[2]Jake Gittlen Laboratories for Cancer Research, Pennsylvania State University College of Medicine, Pennsylvania, USA

[3]Advanced Light Source, Lawrence Berkeley National Laboratory, Berkeley, CA, USA

[4]Department of Biology, Mount Allison University, Sackville, Canada

[5]School of Biosciences, The University of Birmingham, Birmingham, UK

*Equal, contributing corresponding authors:

Khai C. Ang (kca2@psu.edu)

Keith C. Cheng (kcheng76@gmail.com)

Abstract

Daphnia, an emerging model system for the study of evolution, development, phenotypic plasticity, and environmental health, lacks a modern reference atlas for microanatomy. To facilitate the recognition of phenotype caused by the change in genes and environment in the *Daphnia*, we have created the *Daphnia* Histology Reference Atlas (DaHRA, http://daphnia.io/anatomy/). The atlas presents histology of female and male *Daphnia* in three anatomical planes. This interactive web-based resource features overlaid, vectorized annotations that are compliant with an anatomical ontology created for this atlas. We demonstrate the use of DaHRA to contextualize sexual dimorphism in *Daphnia*, and its potential application to the study of tissue toxicity. The web-based documentation of tissue structure can potentially be used in support of unbiased, whole-organism phenotyping in the study of biology and disease.

Introduction

Daphnia is a genus of small planktonic crustaceans with a cyclic parthenogenetic life cycle. It has been a model system in the fields of ecology and evolution (1), often used in studies related to ecotoxicology, phenotypic plasticity, and host-parasite interactions. *Daphnia magna* is one of the most studied species. It primarily inhabits freshwater environments throughout the Northern Hemisphere and is used around the globe as an established invertebrate model in ecotoxicology based on its sensitivity to environmental contaminants that impact its growth, reproduction, mobility, and mortality (2–4). It is widely used to test water quality, has been assigned a role in setting regulatory criteria for toxicity testing by government agencies worldwide (5–8), and has assumed a central role in ecotoxicogenomics (9,10). A comprehensive histology reference atlas is useful to provide normal microanatomical context for histopathological and molecular phenotypes caused by environmental contaminants and stressors.

Histopathology, the histological study of tissue change, permits the identification of cell- and tissue-specific changes associated with toxicity and disease. Its use becomes more powerful for small organisms whose dimensions fit on a histology slide and begins to address the need for unbiased, whole organismal phenotyping in the study of adverse effects of genetic mutations and

31 toxicants (11). The evaluation of toxic effects of chemicals, environmental contaminants, and
32 stressors ideally includes all affected cell types and organ systems to allow a more sensitive and
33 comprehensive understanding of toxic mechanisms. As we know from the fields of medicine (12)
34 and comparative medicine (13), identifying abnormal tissue structure requires prior knowledge of
35 normal structure. Printed histological atlases have been traditionally used to document tissue
36 structure. In the current digital age, web-based reference atlases allow far greater access and
37 flexibility. For example, today's *Caenorhabditis elegans* (http://www.wormatlas.org) (14),
38 zebrafish (http://bio-atlas.psu.edu/) (15), and mouse (https://www.emouseatlas.org/) (16) atlases
39 serve as valuable resources and tools for research and education.
40
41 The web-based histology atlas of *D. magna* (http://daphnia.io/anatomy/) presented here contains a
42 collection of digitized histological images (at 0.25-micron per pixel resolution) of 5-micron thick
43 paraffin sections for adult male and female *D. magna* in the three anatomical planes (coronal,
44 sagittal, and transverse). The interactive atlas viewer displays digital images at user-chosen
45 degrees of magnification with a dynamic scale bar. Manually segmented anatomical structures are
46 highlighted and labeled using an anatomical ontology we created for this atlas. This atlas intends
47 to provide baseline data of normal anatomical and microanatomical structures for the identification
48 of various organs, tissues, and cell-types. Images of a drug-exposed *Daphnia* were included to
49 demonstrate and facilitate understanding of histopathological change. This serves as an example
50 of how the platform might be used for the presentation of experimentally associated phenotypes.
51 We hope this atlas can serve as a foundation to support whole-organism phenotyping associated
52 with genetic and chemical phenome projects related to mutants and exposed animals, respectively.
53

54 Results and discussion

55 The overall strategy of *Daphnia* Histology Reference Atlas (DaHRA) was to design a user-friendly
56 web interface for the presentation of histological data and annotation. We employed routine
57 histology with some adjustments for millimeter-size *Daphnia* (see Material and Methods for
58 details). This involved 1) choosing a fixative that preserves the samples with minimal distortion,
59 and 2) embedding samples in agarose block prepared using a mold. This was done to ensure
60 consistency in sample orientation for histology sectioning in any of the three orthogonal
61 orientations. We processed and sectioned about 100 samples for protocol optimization. Six

samples were labeled for the interactive presentation in the atlas. Figure 1 shows the workflow used to create the atlas.

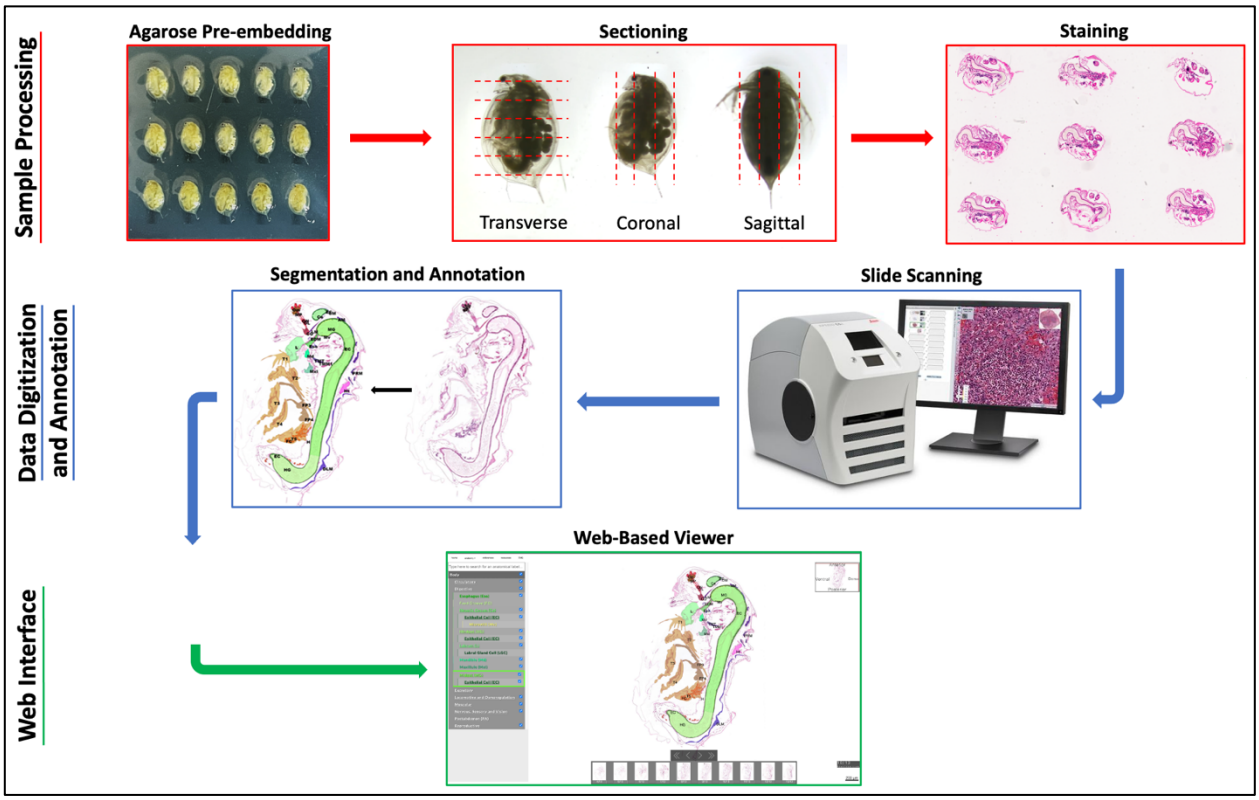

Figure 1. Overall workflow for creating DaHRA. Positioning of fixed *Daphnia* samples was facilitated by agarose embedding prior to paraffin embedding. After processing and sectioning, hematoxylin and eosin-stained slides were digitized, and the best representative images selected for labeling and segmentation of anatomical structures. A web-based viewer was built for the visualization of the annotated images.

Sample processing

Bouin's solution as the fixative of choice for *Daphnia* whole-organism histology

The accurate representation of microanatomy depends upon the preservation of tissue structure with minimal distortion and optimal staining that allows a clear distinction between different cell types and subcellular structures. To determine how to generate sections with minimal distortions for the atlas, we tested three commonly used fixatives: Bouin's solution, 4% Paraformaldehyde in 0.1M phosphate buffer (PFA), and 10% Neutral Buffered Formalin (NBF) (see Materials and Methods). Bouin's and PFA are commonly used to fix *Daphnia*. NBF was also tested because it is the most used fixative for routine histology of mammalian tissues. Overall, the best sections

81 were obtained after fixation in Bouin's solution at room temperature for 48 hours. Bouin's resulted
82 in good gut fixation, allowing microvilli and epithelial cell nuclei to be more distinct (Figure 2A)
83 compared to those fixed with PFA and NBF (Figure 2D and 2G). Nurse cells (nc), oocytes (oo)
84 and yolk granules (yg) are intact in the ovaries (Figure 2B) and cellular features across the
85 developing embryos are also more distinct in samples fixed with Bouin's (Figure 2C).
86
87 A total of 23 *Daphnia* samples were fixed using PFA and NBF, and all showed "ballooning", a
88 severe fixation artifact causing the carapace to 'puff-up' (S1 Figure). Inconsistent tissue
89 preservation and distortion in some microanatomical structures were also observed. Particularly,
90 the epithelial cells are not as distinct, and the microvilli are generally not visible in the gut (Figure
91 2D and 2G). In the ovaries, oocytes and nurse cells are not intact and hardly distinguishable (Figure
92 2E and 2H)., The developing embryos also showed less cell clarity (Figure 2H and L). In sum,
93 Bouin's solution was observed to be the best fixative for *Daphnia* whole-organism histology and
94 was used to fix all samples used in this atlas.
95

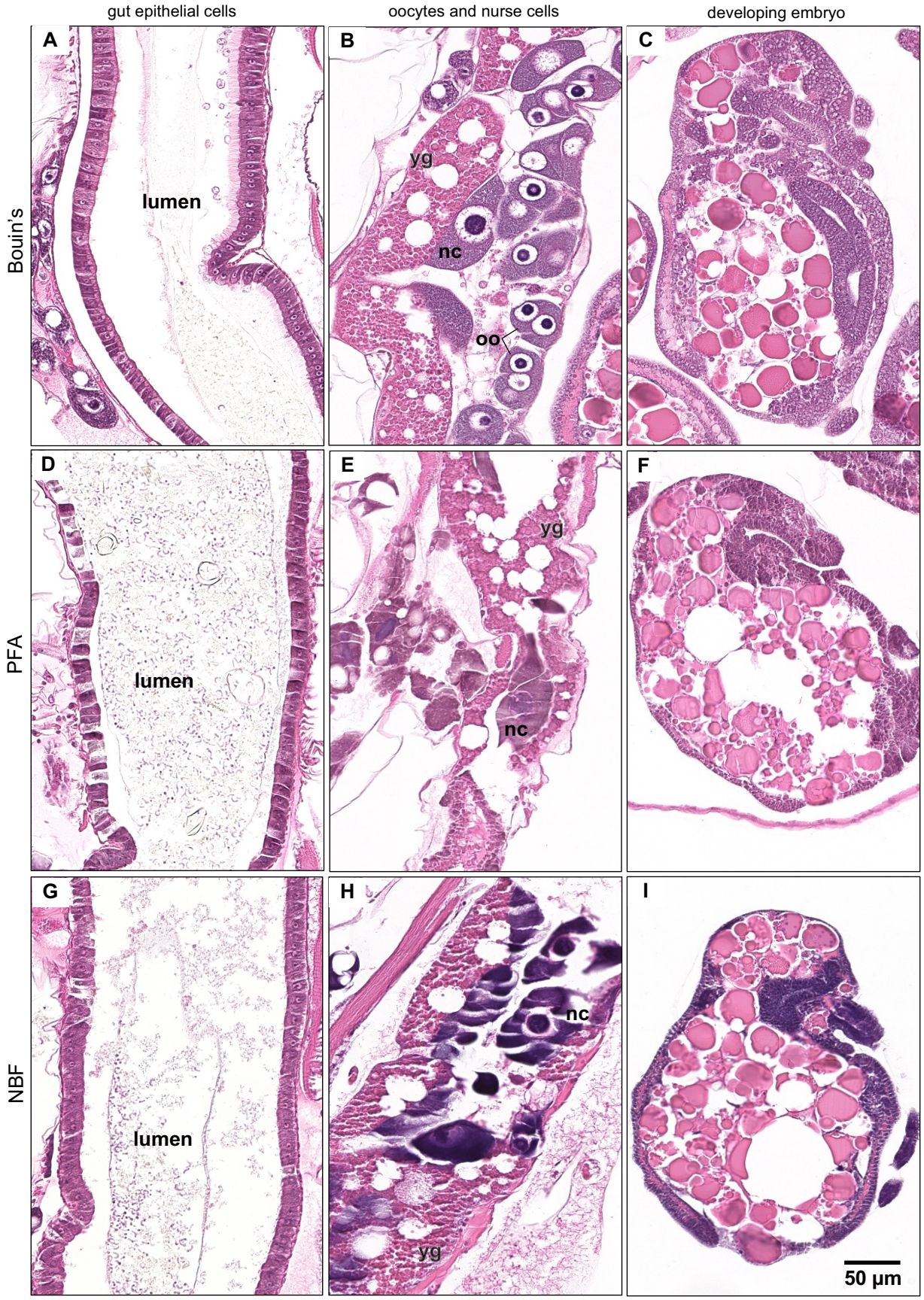
gut epithelial cells
oocytes and nurse cells
developing embryo
Bouin's
PFA
NBF
A
B
C
D
E
F
G
H
I
lumen
yg
nc
oo
50 µm

Figure 2. Comparison of histological sections generated from samples fixed with Bouin's (A-D), PFA (E-H) and NBF (I-L). Bouin's fixed samples resulted in good gut fixation, allowing microvilli and epithelial cell nuclei to be more distinct compared to those fixed with PFA and NBF. Nurse cells (nc), oocytes (oo) and yolk granules (yg) were more intact in the ovaries of samples fixed with Bouin's. Cellular features across the developing embryos are also more distinct in samples fixed with Bouin's. Full size images of each panel are available in Supplemental S2A-I Figures.

Agarose pre-embedding using a casting mold enables consistent sample orientation

Visualization of anatomical sections in each of the three standard anatomical planes (coronal, sagittal, and transverse) is critical for understanding organismal anatomy. Therefore, the ability to generate consistent sections in each of the planes is essential. Agarose pre-embedding using mold or array facilitates consistent position and orientation of millimeter-size samples for sectioning (15,17). We have taken that same approach here, using custom-designed plastic mold to create agarose blocks with wells that hold individual fixed *Daphnia* samples prior to tissue processing and paraffin embedding. We tested several designs of casting molds (S3 Figure) and found that agarose blocks cast using triangular mold (Figure 3, STL file in S1 File) allowed precise positioning of adult *D. magna* samples with ease (see Materials and Methods for details). Using the mold for agarose pre-embedding, we were able to embed up to 18 samples per paraffin block for sectioning.

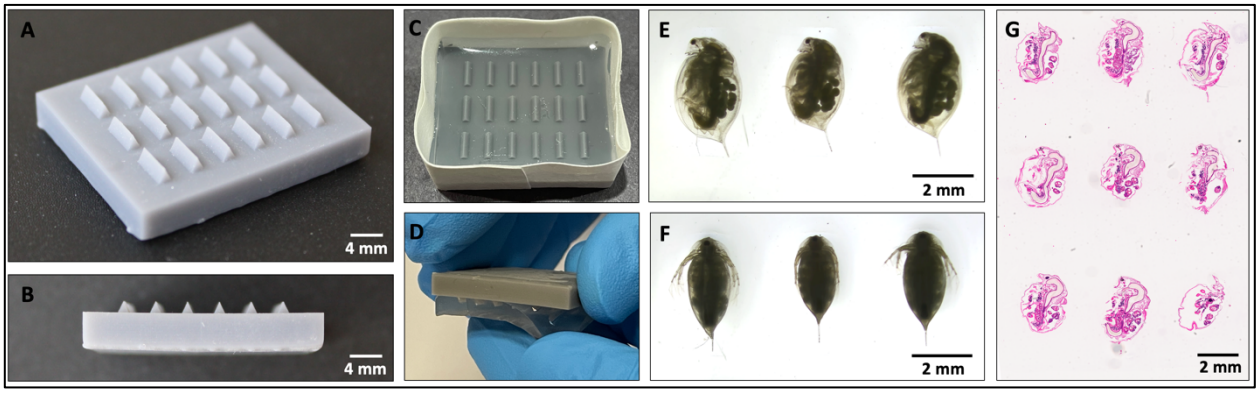

Figure 3. Agarose embedding using casting mold to ensure better positioning of *Daphnia* samples for histology sectioning. (A) Top view and **(B)** side view of triangular mold printed by stereo-lithography (3D-SLA) at 25 µm resolution for a smooth surface allowing easy removal of agarose block. **(C)** Casting 1% agarose block in the taped mold. **(D)** Agarose block being removed from the mold after solidification by peeling the gel downwards. **(C)** *Daphnia* samples were laid

on their sides with a swimming antenna in the wells, the rostra facing the same direction for sagittal plane sectioning, and **(F)** laid on their back in the wells for coronal and transverse plane sectioning. **(G)** The histological section showed the position of samples at a similar plane.

Data digitization and annotation

Slide scanning and image processing for background removal

After hematoxylin-eosin staining, all slides were viewed under microscope using 20X and 40X objective lenses and screened for samples having sections with least distortion and best representing the overall microanatomy. Selected slides were scanned using an Aperio AT2 slide scanner (see Materials and Methods for details), yielding images with 0.25-micron per pixel images. For the best presentation of images on the atlas, image processing was performed manually to remove background of the selected digital slide. The region of selected samples was first extracted using Aperio ImageScope (version 12.4.3.5008). Three channels (Red, Green, Blue) of these images were stacked using Fiji or ImageJ and saved as a TIF format. After background removal using Adobe Photoshop, each set of digital slides was then pyramidally tiled to deepzoom format using libvips (18) in preparation for the web-based viewer.

Terminology for anatomical ontology and digital segmentation of anatomical structures for DaHRA

To ensure the terminology used for DaHRA anatomical ontology (a list of terms organized by groups and subgroups) that we created is consistent and relevant with current research, we cross-referenced the extensive work of Fryer (19) with other published literature (20–46) and decided on the commonly used *Daphnia*-specific terms. We were able to identify 50 anatomical structures. To simplify visualization, we categorized them into 8 groups (circulatory, digestive, excretory, locomotive and respiration, muscular, nervous, sensory and vision, post-abdomen and reproductive) and assigned color to each structure based on the grouping (S2 File). Each anatomical structure was labeled and segmented by outlining the structure with the curvature tool in Adobe Illustrator to enable interactive highlighting of anatomical structures on the atlas.

Web interface

Interactive viewer for DaHRA

The goal of DaHRA is to provide user-friendly access to a collection of digitized histological sections generated from serially sectioned wildtype *D. magna* of both sexes in three standard anatomical planes (Figure 4). Toxicological data is hosted under a separate landing page which can be viewed under “Histopathology” tab.

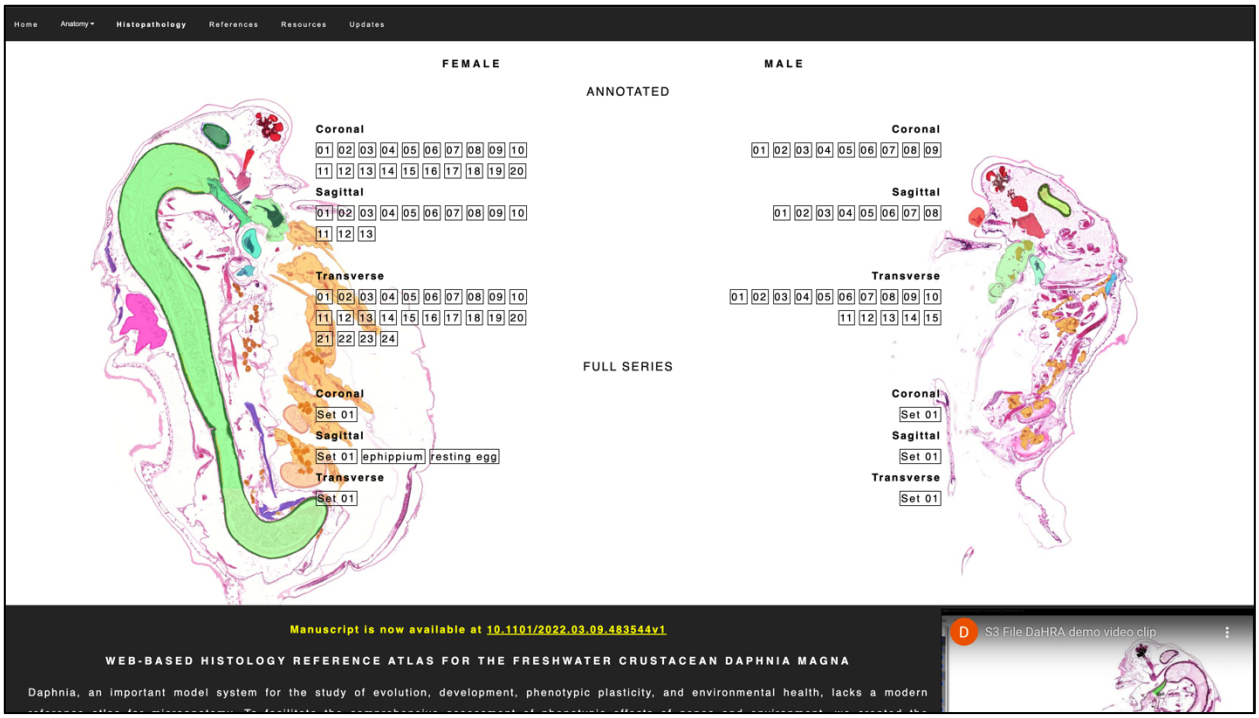

Figure 4. Landing page of DaHRA containing annotated and unannotated histology images of female and male *D. magna* with a short instruction video explaining the features of the atlas.

Clicking on any thumbnails under “Annotated” on the anatomy landing page will lead users to the viewer that combine digital scans (0.25-micron per pixel resolution) with annotations. In the viewer, the anatomical ontology is listed on the left, arranged in a hierarchical tree that can be expanded and collapsed (Figure 5). Annotations of the structures are presented as color overlays and indicated by a check mark in the box next to the anatomical term. Unchecking the box temporarily hides the color overlays. Anatomical terms with underlined labels indicate that there is at least one nested substructure (for example, “microvilli” under “epithelial cell”, both under “midgut"). Hovering over an anatomical term in the ontology dynamically highlights the

corresponding structure or structure groups in the viewer, temporarily hiding other checked structures. The search function above the ontology can also be used to find structures.

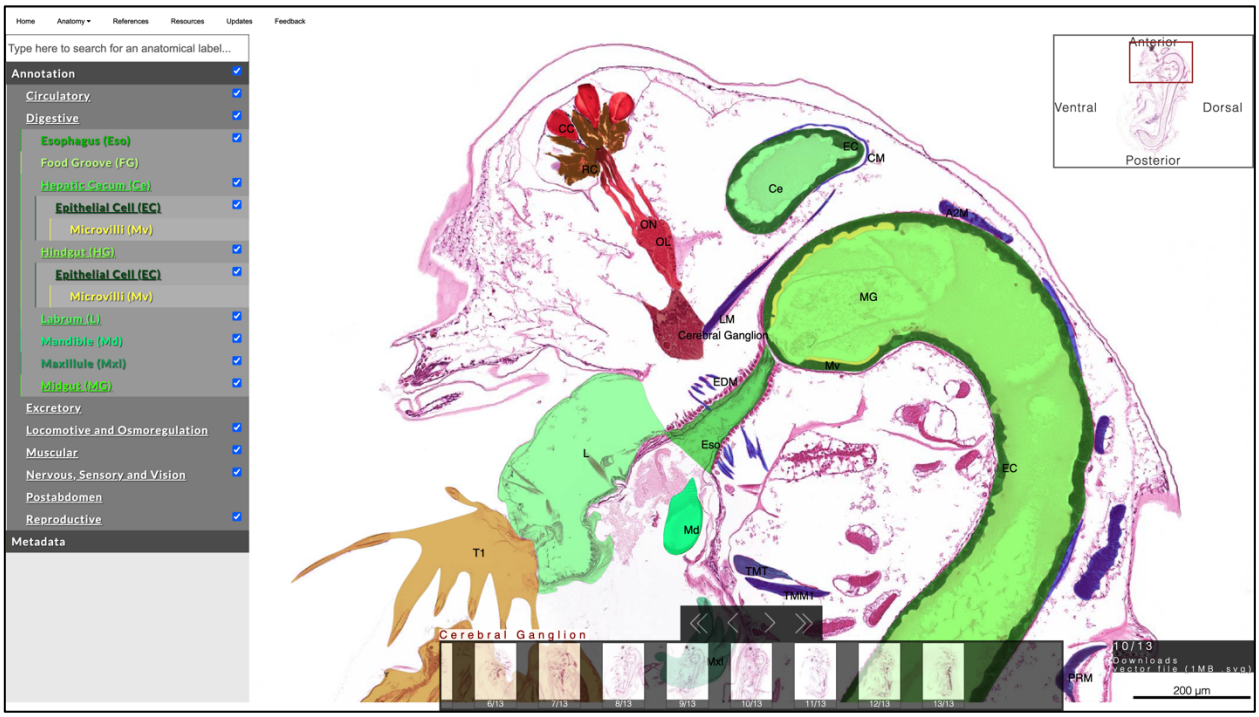

Figure 5. Overview of the interactive web-based viewer for DaHRA. The left pane of the viewer includes an expandable hierarchical tree of anatomical structures; the checked boxes indicate which structures are labeled in the image. The image shows acronym labels; hovering the mouse cursor over an acronym or its corresponding region will bring up the structure's full name. Unchecking a box will eliminate the corresponding color overlay and annotation.

On the histology image, all available color overlays and acronym labels are on display by default (individually indicated by checked checkboxes in the ontology) (Figure 5). Full name of a structure will be displayed by hovering the cursor over a colored region. Clicking on the colored region will change the colored overlay to only highlighting the border. While selected sets of histology images with interactive highlighting were presented in the atlas, additional unannotated images of serially sectioned *D. magna* are also available and categorized under 'Full Series'. All the files (.ai, tiff, SVG) for the atlas are also available for download.

The "Resources" tab contains a list of anatomical definition and all the protocols used to generate this atlas. The "Reference" tab lists published literature used for the anatomical annotations. The "Updates" tab will list all the updates to datasets and viewer. To enable collaborative effort with

196 the scientific community, keep the atlas relevant to scientific progress and ensure the accuracy of
197 the atlas content, the "Feedback" tab provides a platform for users to leave comments and
198 suggestions. A video clip demonstrating the features of the atlas (S3 File) can be also found on the
199 anatomy landing page of this atlas.
200

201 *Daphnia magna* anatomy

202 Studies of *Daphnia* functional anatomy, physiology, and development are extensive, but histology
203 images are not widely available. DaHRA presents the first extensive collection of images for both
204 sexes of *D. magna* in an annotated visualization platform for interrogating *Daphnia* anatomy. All
205 organs and cell types included in the anatomical ontology are briefly described here with
206 representative images from the three anatomical planes of females (Figure 6A-C) and males
207 (Figure 6D-F).
208

209 Circulatory

210 *Daphnia* have an open circulatory system and a myogenic heart (39,40). The heart (Ht) has a pair
211 of ostia situated to the immediate anterior of the brood chamber, between the midgut and dorsal
212 surface (Figure 6B, 6C, 6F). As *Daphnia* are semi-transparent, the beating heart can be easily
213 observed. Hemolymph (blood-like fluid) containing hemocytes (H) or blood cells (Figure 6C
214 inset) (21,35) is pumped through the body cavity.
215

216 Digestive

217 *Daphnia* are filter feeders. Food particles are filtered through filter plates (FP3 and FP4) consisting
218 of setae on thoracic limbs 3 and 4, passed through maxillules (Mxl) and mandibles (Md) into the
219 esophagus (Eso), which is the first part of the digestive system (Figure 6A and B). The digestive
220 system also consists of paired hepatic ceca (Ce), midgut (MG), and hindgut (HG) (Figures 6A-C,
221 6E-F) that are lined with epithelial cells and microvilli, with the columnar epithelial cells in the
222 midgut, and the cuboidal cells in hepatic ceca and hindgut (37,41). The labrum (L) houses labral
223 gland cells (LGC) that have been suggested to be involved in food ingestion and endocrine function
224 (45,46) (Figure 6B-D).
225

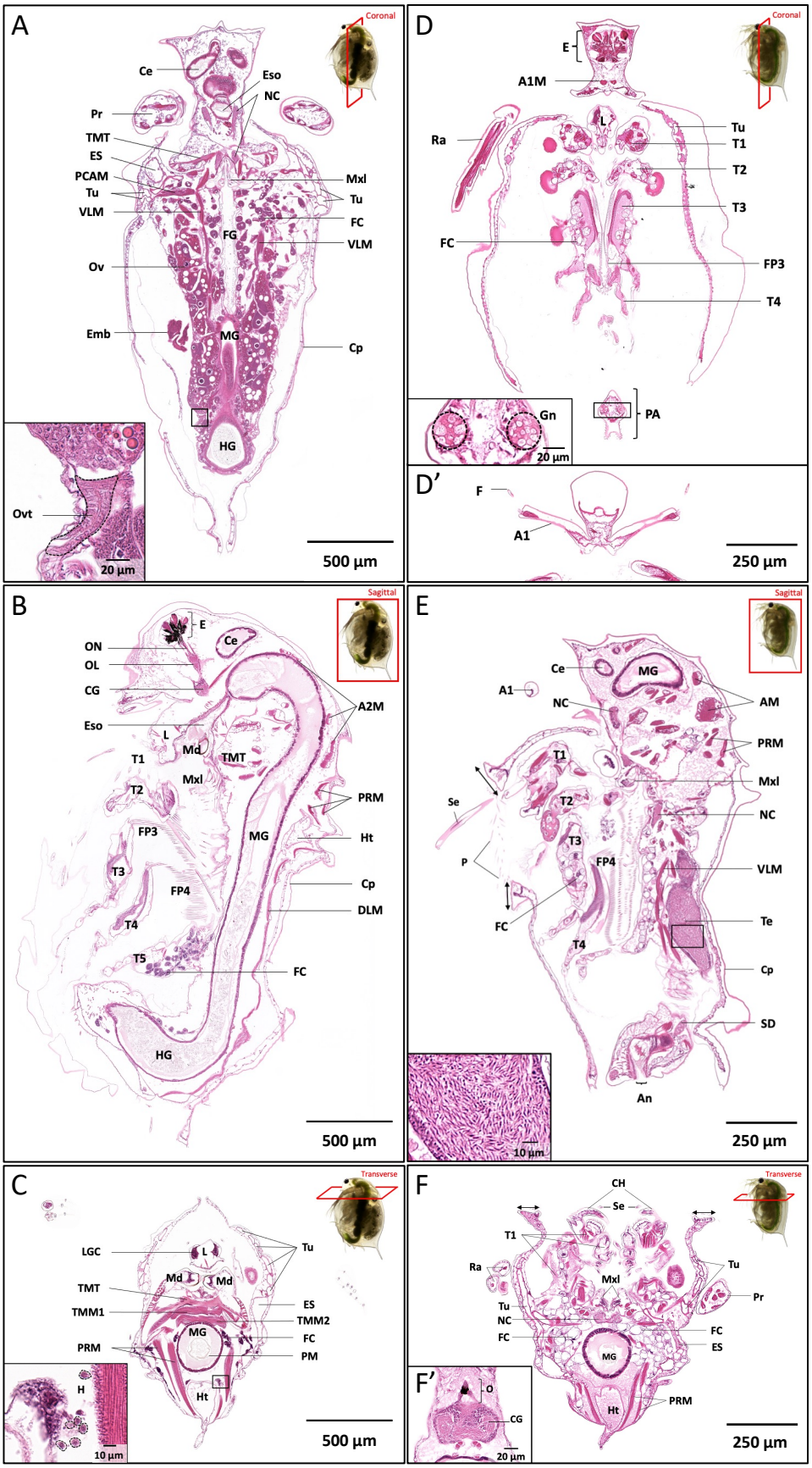
A
Coronal
Ce
Eso
NC
Pr
TMT
ES
PCAM
Tu
VLM
Mxl
Tu
FC
FG
VLM
Ov
Emb
MG
Cp
HG
Ovt
20 µm
500 µm
D
Coronal
E
A1M
L
Ra
Tu
T1
T2
T3
FC
FP3
T4
Gn
20 µm
PA
D'
F
A1
250 µm
B
Sagittal
E
Ce
ON
OL
CG
A2M
Eso
L
Md
T1
TMT
Mxl
T2
PRM
FP3
MG
Ht
T3
FP4
Cp
DLM
T4
T5
FC
HG
500 µm
E
Sagittal
Ce
MG
A1
NC
AM
PRM
T1
Mxl
Se
T2
NC
T3
P
FP4
VLM
FC
Te
T4
Cp
SD
An
10 µm
250 µm
C
Transverse
LGC
L
Tu
Md
Md
TMT
ES
TMM1
TMM2
MG
FC
PRM
PM
H
Ht
10 µm
500 µm
F
Transverse
CH
Se
T1
Ra
Tu
Mxl
Pr
Tu
NC
FC
FC
ES
MG
F'
O
CG
20 µm
Ht
PRM
250 µm

Figure 6. Representative images showing anatomical structures of female (A-C) and male (D-F') *D. magna* in the three orthogonal planes. The coronal plane (panel A and D) displays most of the structures in pairs. Inset of panel A shows the oviduct (Ovt; dotted circle) and inset of panel D shows gonopores (Gn) in the male. Panel D', slightly ventral to panel D, displays the prominent and elongated antennules (A1) with flagella (F) at the tip. The sagittal plane of the female (panel B) displays the connection of the compound eye (E) to the optic lobe (OL) and cerebral ganglion (CG) by optic nerves (ON). The labrum (L), maxillules (Mxl), and mandibles (Md) are anterior to the esophagus (Eso) that opens into the midgut (MG) and is followed by the hindgut (HG). This section also cuts through the five thoracic limbs (T1-5) and filter plates (FP3, FP4). The sagittal plane of the male (panel E) shows the elongated seta (Se) on the first thoracic limb, pubescence (P) at the wider ventral opening of the carapace, thickening of carapace at the ventral opening (arrows), one of the testes (Te), and a small portion of sperm duct (SD). Inset of panel E showing the spermatozoa in the testis. The transverse plane of the female (panel C) shows the asymmetrical paired mandibles (Md) with the transverse mandibular tendons (TMT), transverse mandibular muscles (TMM1), transverse muscles of mandibles (TMM2), and the posterior rotator muscles of mandibles (PRM). Inset of panel C displays several hemocytes (H) outlined by dotted circles. The transverse plane of male (panel F) displays the paired copulatory hooks (CH) on the first thoracic limbs (T1) and the thickening of the carapace (arrows) at the ventral opening. This also shows the abundance of fat cells (FC) which are quite different from those in the female. Panel F', slightly above that of panel F, shows the pigmented ocellus (O) is connected to the cerebral ganglion (CG). A1M, antennule muscle; A2M, antennal muscle; An, anus, Ce, hepatic cecum, Cp, carapace; DLM, dorsal longitudinal muscle; ES, end sac of the maxillary gland, FG, food groove; Ht, heart; LGC, labral gland cell; NC, nerve chord; PA, postabdomen; PCAM; posterior carapace adductor muscle; PM, peritrophic membrane; Ra, ramus of swimming antenna; Tu, tubule of the maxillary gland, VLM, ventral longitudinal muscle. Corresponding atlas links:
A) https://daphnia.io/anatomy/histology/?t=coronal_female&z=10
B) http://daphnia.io/anatomy/histology/?t=sagittal_female&z=10
C) http://daphnia.io/anatomy/histology/?t=transverse_female&z=10
D) https://daphnia.io/anatomy/histology/?t=coronal_male&z=4
D') http://daphnia.io/anatomy/histology/?t=coronal_male&z=2&c=0.2,0.14,0.6,0.4
E) http://daphnia.io/anatomy/histology/?t=sagittal_male&z=3
F) https://daphnia.io/anatomy/histology/?t=transverse_male&z=8
F') http://daphnia.io/anatomy/histology/?t=transverse_male&z=4&c=0.43,0.25,0.18,0.12

Excretory

The maxillary gland, also known as the shell gland, is the organ of excretion, housed between the inner and outer walls of the carapace (38). It consists of an end sac (ES), a series of tubules (Tu), and an opening that is situated within the anterior part of the brood chamber (Figure 6A, C, D and F).

Locomotive and osmoregulation

The second pair of antennae, also referred to as swimming antennae, is the primary organ of locomotion. Each swimming antenna has a protopodite (Pr), two rami (Ra) bearing setae (20)(Figure 6C, D, and F), and is supported by antennal muscles (A2M). *Daphnia* has five thoracic limbs (T1-T5) (23) (Figure 6B, D, and E). Movements of thoracic limbs produce a constant current that brings food particles into the digestive tract (19,22) and facilitates osmotic regulation, which occurs in the epipodite on each thoracic limb (32). First thoracic limbs in male are different from the female *Daphnia*, with only the male having the chitinized copulatory hooks (CH) (Figure 6F) and longer setae (Se) (Figure 6E).

Muscular

The muscular system is very prominent and occupies a significant portion of the body (19,24). The largest muscles are ventral and dorsal longitudinal muscles (VLM and DLM) that extend along the gut, three paired antennal muscles (A2M), transverse mandibular muscles (TMM1), transverse muscles of mandibles (TMM2), posterior rotator of the mandibles (PRM), carapace adductor muscles (ACAM and PCAM), and followed by groups of muscles that allow the motion of thoracic limbs and postabdomen (Figure 6). Other small muscles include those around the compound eye (26), labrum, and esophagus. All muscles are striated and surrounded by sarcoplasm, which contains many nuclei and is mostly vacuolated. Sarcoplasm is particularly abundant and more vacuolated in the antennal muscles.

Nervous, sensory, and vision

Daphnia has a pigmented compound eye (E) consisting of 22 ommatidia, derived from two eyes that fuse after embryonic development, and a small, pigmented ocellus (O) with three lens-like bodies (Figure 6F'). The optic nerve (ON) of each ommatidium forms a parallel bundle that connects to the optic lobe of the cerebral ganglion (OL), which is then connected to the cerebral ganglion (CG) (Figure 6B). The cerebral ganglion is connected to two chains of nerve cords (NC) that run along the thorax, underneath the gut, and reach other anatomical structures (33,34,42) (Figure 6A, E, and F). Male has prominent and elongated first antennae or antennules (A1), uniquely with flagella (F) at their tips (Figure 6D').

Reproductive

The ovaries in females (Figure 6A) and the testes in males (Figure 6E) are paired and situated ventrally along the gut. *Daphnia* and all other species under the order Cladocera are cyclical parthenogens, which involve both sexual (meiotic) and clonal (ameiotic) reproduction (47). Under favorable environmental conditions, females reproduce parthenogenetically, and broods of genetically identical embryos will develop in the brood chamber before being released. Sexual reproduction is cued by environmental stress (often seasonal, including photoperiod, temperature, and over-crowding) that triggers the production of genetically identical males instead of females. During this sexual phase of the *Daphnia* life cycle, females also switch to producing two haploid eggs. Unlike parthenogenetic embryos, the development of these sexually produced embryos is arrested at the 3000-cell stage (48) and enter into a state of dormancy while being encased within an ephippium that protects these embryos under diapause through harsh environmental conditions for decades and even centuries (49,50). These two 'resting eggs' are different from parthenogenetically produced eggs that can number up to 100 per brood. Parthenogenetic eggs contain multiple oil droplets (od) of varying size and yolk granules (yg) that are generally larger in size (31) (Figure 7). Images of *Daphnia* in sexual reproduction ('ephippium' and 'resting eggs') can be found under "Full Series" on the atlas.

Testes of male *Daphnia* consist of two long tubular structures connected to gonopores (Gn) or ejaculatory openings by sperm ducts (Figure 6D and E). Spermatogenesis begins at the testes' walls, and mature spermatozoa are displaced inward toward the central region of the testes (43).

Fat cells, which are polyploid (51) and consist of a massive portion of lipid and glycogen (44), are abundant in healthy *Daphnia*. They are found along the gut, on the thoracic limbs, and around ovaries or testes (Figure 6). These cells are most likely sites of the vitellogenin synthesis (44). They have been implicated with the epipodite cells (on thoracic limbs) in the synthesis of hemoglobin (29).

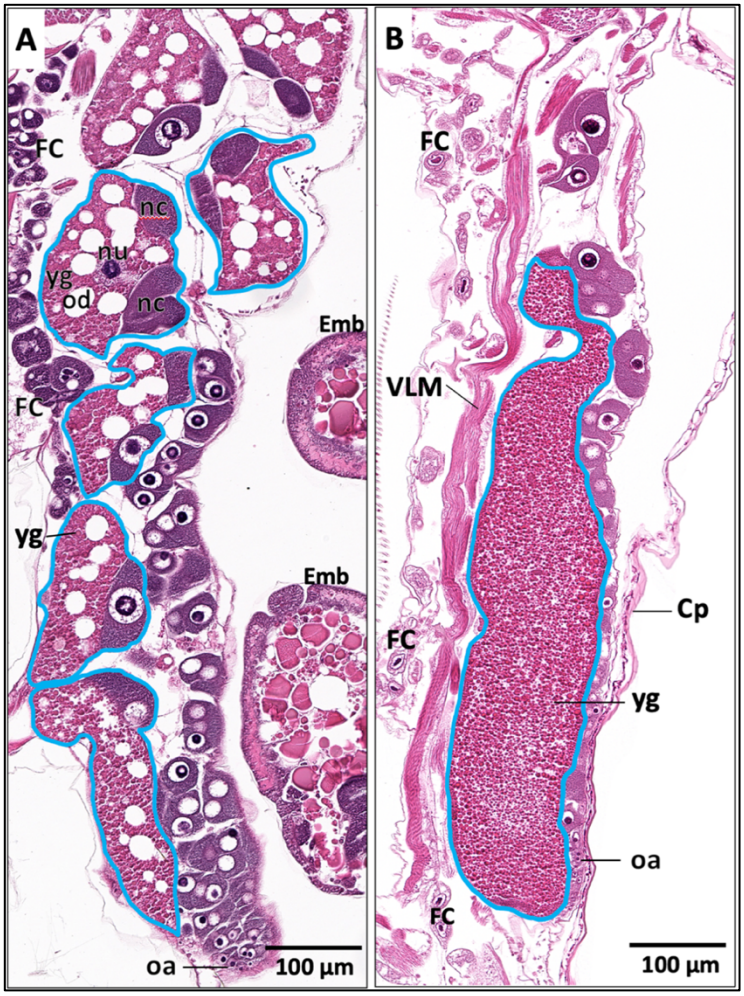

Figure 7. Comparison of ovarian eggs in females reproducing parthenogenetically or sexually. (A) The ovarian eggs of a female reproducing parthenogenetically contain a large amount of oil droplets (od) and yolk granules (yg) that are generally larger in size. **(B)** The ovarian egg of a female reproducing sexually contains a large proportion of fine yolk granules without oil droplets. Cp, carapace; Emb, embryo; FC, fat cell; nc, nurse cell; nu, the nucleus of oocyte; Oa, oogonia; VLM, ventral longitudinal muscle. A solid blue circle indicates an individual ovarian egg.

Sexual dimorphism

Multiple forms of sexual dimorphism in *Daphnia* are present outside the reproductive system. Due to the predominantly parthenogenetic life cycle of *Daphnia*, there is less information on male anatomy in contrast to the females. Our atlas provides the first detailed collection of histology images of male *Daphnia*. Briefly, sexual dimorphism in *Daphnia* includes smaller male body size and male prominence and elongation of antennules (A1), uniquely with flagella (F) at their tips (Figure 6D'). Male antennules carry muscles (A1M) (Figure 6D) that are absent in the females.

The first thoracic limbs of the males are equipped with elongated setae (Figure 6E) and chitinized copulatory hooks (Figure 6F) that are used for clasping females during copulation. The male post-abdomen has gonopores (Figure 6D inset) that are involved in transferring mature spermatozoa from the testes to the female in the region of the oviduct during copulation. Besides having a wider opening at the ventral margin of the carapace, thickened and angular margins (indicated by arrows in Figures 6E and F) are observed around the hairy opening in males. One of the male-specific traits clearly illustrated in our atlas is that fat cells in males are comparatively different from those in females. Fat cells in males contain much larger lipid droplets, reduced and less granular cytoplasm, and smaller nucleoli that are usually situated at the periphery of the cell (Figure 8).

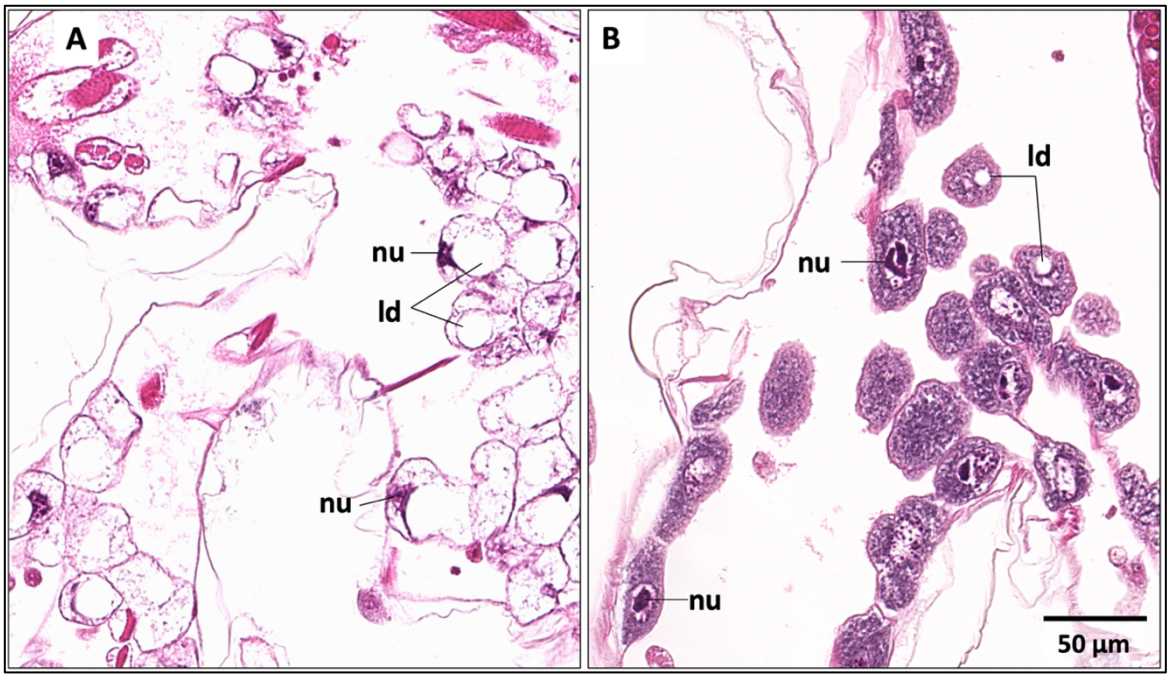

Figure 8. Comparison of male and female fat cells. (A) Fat cells in the male consist of larger lipid droplets (ld), reduced and less granular cytoplasm with smaller nucleoli (nu) that are situated at the cell periphery. **(B)** Fat cells in the female have more granular cytoplasm with smaller lipid droplets (ld) and bigger nucleoli (nu).

Documenting histopathological change using DaHRA

To illustrate how whole-organism digital atlasing facilitates understanding of abnormal tissue architecture in the context of the whole organism, we share an example of how the atlas helps us to identify pathological tissue phenotypes associated with a chemical exposure.

364 Adult pregnant *D. magna* carrying third brood of embryos (about two hours post-ovulation) were
365 exposed to an over-the-counter pain reliever for 72 h and processed using the workflow described
366 in Material and Methods. Dead and severely deformed embryos were noted in the brood chamber
367 by dissecting microscope. While presenting a complete set of experiments lies beyond the scope
368 of this paper, the representative exposed animal shown on the atlas under "Histopathology" tab
369 illustrates the potential use of web-based comparisons of histology between wildtype and the
370 exposed animals can be used to enhance identification of microanatomical phenotypes.
371
372 Histology of whole-organism sections revealed changes in various organs and cell types besides
373 the dead and deformed embryos in the brood chamber. The severely deformed embryos remained
374 in chorion with some development of the compound eye and gut precursor but no visible
375 development of the swimming antennae or thoracic limbs (Figure 9E). Vacuolation (indicated as
376 V) was observed in most fat cells (Figure 9H) and across the digestive system, including the labral
377 gland cells (Figure 9F), midgut (Figure 9G) and hindgut (Figure 9H). The midgut and hindgut of
378 the exposed *Daphnia* also showed excessive sloughing or shedding of degenerated epithelial cells
379 (Figure 9G and H).
380
381 Reproductive, behavioral and physiological parameters are more commonly used for the
382 evaluation of toxicity effects in *Daphnia* (3). Few toxicological studies employed ultrastructural
383 analysis of a target organ, usually just the midgut, for the histopathological examination (52–55).
384 Our observation of alterations and histopathological changes in developing embryos, fat cells and
385 labral gland cells, other than the whole digestive tract (ceca, midgut, and hindgut) in the exposed
386 *Daphnia* demonstrated that the assessment of toxic effects should be of non-targeted and unbiased.
387 Screening for morphological phenotypes should be done ideally from slides encompassing the full
388 cross-section of the organism to facilitate unbiased evaluation across all organ systems for the full
389 range of phenotypes.

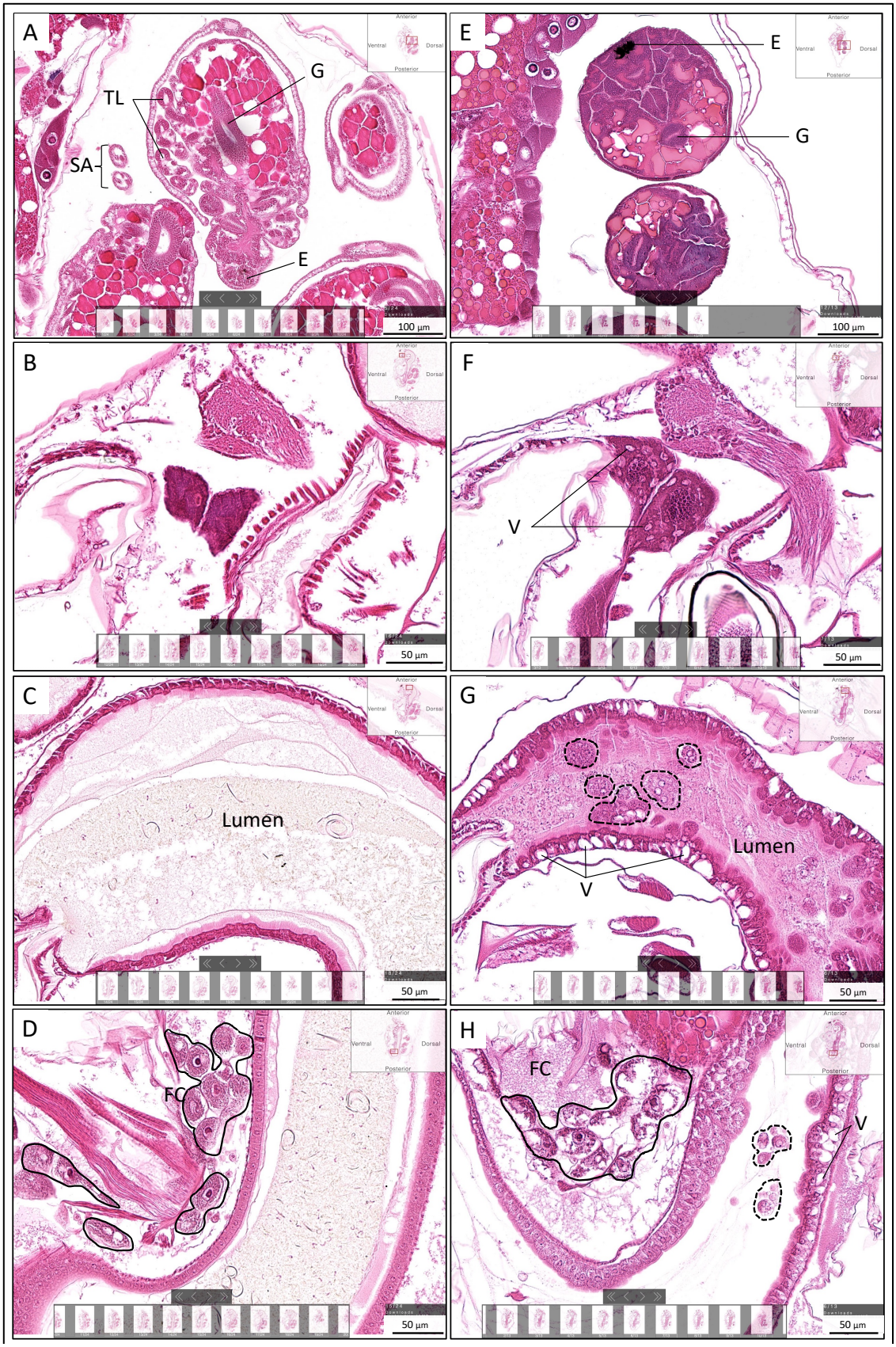
A
TL
G
SA
E
100 µm
E
E
G
100 µm
B
50 µm
F
V
50 µm
C
Lumen
50 µm
G
Lumen
V
50 µm
D
FC
50 µm
H
FC
V
50 µm

390

Figure 9. Pathological changes were observed across organ systems in a drug-exposed *Daphnia* (E-H) as compared to the wildtype (A-D). (E) Severely deformed embryos with some development of the compound eye (E) and gut (G) precursor but no visible development of the swimming antennae (SA) and thoracic limbs (TL). **(F)** Vacuoles (V) are observed in the labral gland cells. **(G)** Vacuoles (V) and sloughing of degenerated epithelial cells (dotted circles) are observed in the midgut. **(H)** Alteration observed in the fat cells (FC) at the post-abdomen region and vacuoles (V) and sloughing of degenerated epithelial cells (dotted circles) are observed in the hindgut. Corresponding atlas links:

(A) http://daphnia.io/anatomy/histology/?t=sagittal_female_64&z=5&c=0.503,0.595,0.324,0.310
(B) http://daphnia.io/anatomy/histology/?t=sagittal_female_64&z=16&c=0.29,0.277,0.187,0.179
(C) http://daphnia.io/anatomy/histology/?t=sagittal_female_64&z=18&c=0.474,0.192,0.24,0.22
(D) http://daphnia.io/anatomy/histology/?t=sagittal_female_64&z=15&c=0.32,1.02,0.18,0.16
(E) http://daphnia.io/anatomy/histology/?t=sagittal_female_common_pain_reliever&z=12&c=0.48,0.64,0.31,0.26
(F) http://daphnia.io/anatomy/histology/?t=sagittal_female_common_pain_reliever&z=7&c=0.35,0.32,0.18,0.15
(G) http://daphnia.io/anatomy/histology/?t=sagittal_female_common_pain_reliever&z=6&c=0.46,0.27,0.22,0.18
(H) http://daphnia.io/anatomy/histology/?t=sagittal_female_common_pain_reliever&z=6&c=0.34,0.96,0.22,0.18

Conclusions and future directions

Compared to other model organisms (zebrafish, mouse), histological data of *Daphnia* is not yet widely available. This led to the creation of DaHRA, an open-source visualization platform of *Daphnia* normal histology as an educational tool and scientific resource. A drug-exposed *Daphnia* was included in the atlas illustrating histopathological change that can be characterized across organs and cell types. This also demonstrated that screening for morphological phenotypes and the assessment of toxicity should ideally be of non-targeted, unbiased and in a whole-organism context. Through collaboration and additional resources, datasets covering major developmental stages, and morphological and pathological change caused by environmental pollutants, stressors, and genetic variation can be added.

Multimodal imaging is providing opportunities for more comprehensive understanding of anatomy and microanatomy (56,57). Advances in 3D imaging, such as 3D fluorescence (58,59) and X-ray tomography (60,61) enables the measurement and quantitative analysis of 3D microanatomy that is lacking in histology. The next phase of creating a 3D atlas will take extensive, separate work but is most useful when linked with corresponding histological images. Histological images such as those provided by DaHRA are useful for the confirmation of tissue details and cell types in the gray-scale x-ray tomographic slices (Figure 10). Notably, the understanding of structures from

both 2D and 3D imaging modalities will require inspection of 2D images, which can benefit from our atlas labeling and visualization tools (Figure 10C).

The use of shared infrastructure for web-based atlases across animal models is needed to facilitate comparisons between species and multi-modal data (62). Ideally, the open-source tools of DaHRA can be applied to other model organisms and potentially contribute to the cross-phylogenetic atlases. Cross-phylogenetic atlases may be used to support the goals of comparative pathology and cross-model organism validation for diseases as prioritized by the National Institutes of Health (62), and may also be useful for toxicology and characterization of the diversity of life.

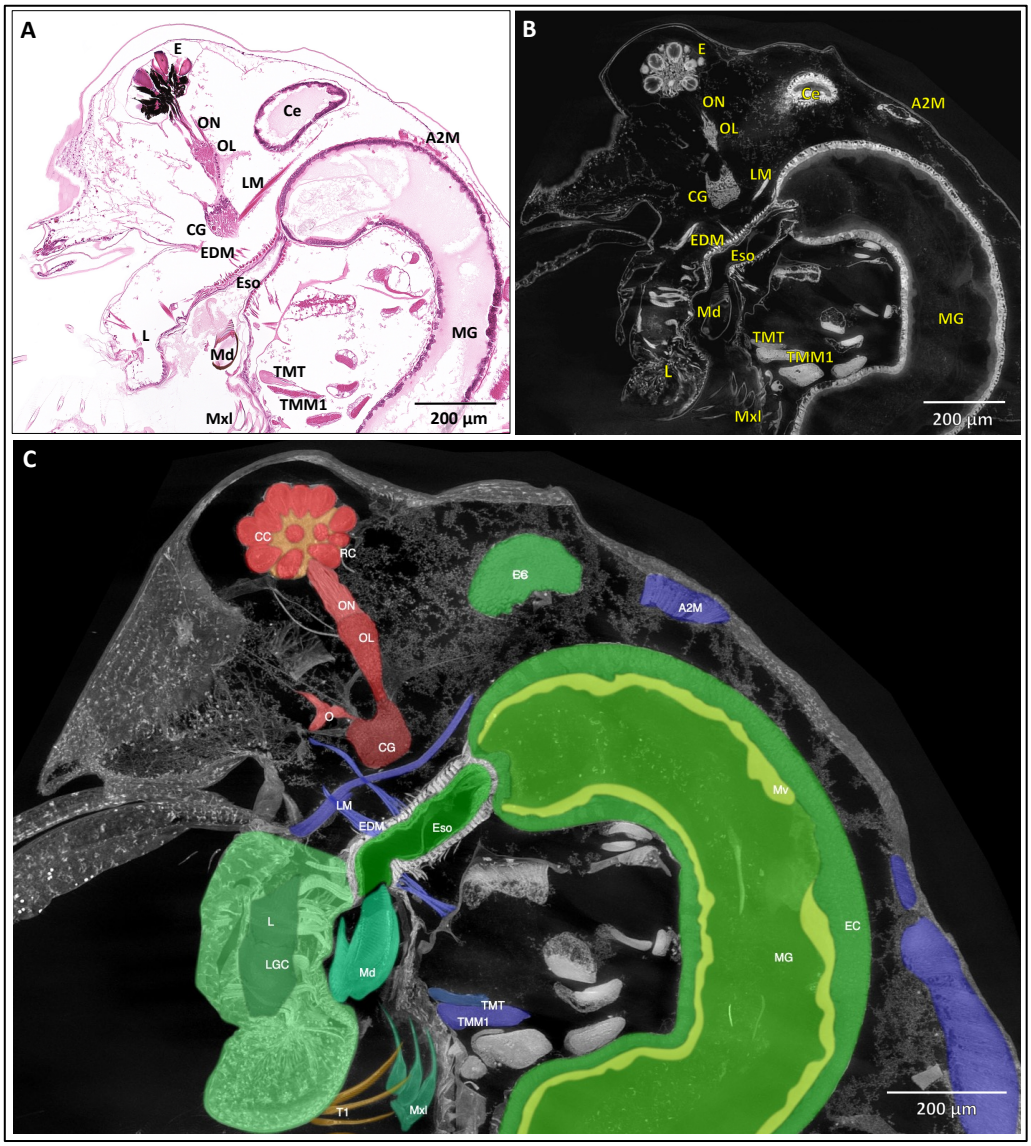

Figure 10. Cross-referencing of histology with microCT-based X-ray tomography. (A) The anatomical structures of a female *D. magna* in a 5-micron histology section, cross-referenced with **(B)** a 0.5-micron x-ray tomographic slice. **(C)** Color-overlay highlighting in the 25-micron x-ray tomographic stack corresponding to panel B, provides more spatial context of various anatomical structures, available in the atlas at http://daphnia.io/anatomy/histotomography/?t=AAA392&z=1&c=0.18,0.02,0.79,0.55. A2M, antennal muscle; Ce, hepatic cecum; CC, crystalline cone of ommatidium; EDM, esophageal dilator muscle; Eso, esophagus; L, labrum; LGC, labral gland cell; LM, levator muscle of labrum; Md, mandible; Mv, microvilli of midgut; Mxl, maxillule; MG, midgut; O, ocellus; OL, optic lobe of cerebral ganglion; ON, optic nerve; TMM1, transverse mandibular muscle; TMT, transverse mandibular tendon.

Material and methods

Daphnia magna husbandry

Daphnia magna were purchased from Carolina Biological (NC, USA) and raised in "Aachener Daphnien-Medium" or ADaM (61) with modified content of selenium at room temperature (20°C ± 1°C) under a 16-hour light/8-hour dark photoperiod. *D. magna* were fed three times weekly with 3.0 x 10^7 cells/ml of green microalgae (*Raphidocelis subcapitata)* and 0.1 mg/mL of dissolved bakers' yeast. The animal density was maintained at about 20 neonates, 10 juveniles and 6 to 8 reproducing adults per liter to prevent overcrowding and trigger the production of resting eggs and male *D. magna*. Under these conditions, animals reached maturity 6 to 8 days post-birth and reproduced parthenogenetically every 3 days with an average of 15 neonates per brood from the second brood onwards. Production of males and females carrying resting eggs was induced by overcrowding (>10 reproducing adults per liter) and shorter photoperiod (10 h).

Fixation and decalcification

Daphnia magna were euthanized in glass vials filled with bicarbonate water. Live *D. magna* were transferred using plastic transfer pipettes. Tips of transfer pipettes were trimmed at a 45° angle such that the diameter was double the size of the samples. Immediately following euthanasia, bicarbonate water was gently removed with a transfer pipette and replaced with at least 20X specimen volume of Bouin's solution (Newcomer Supply, WI), 4% Paraformaldehyde in 0.1M phosphate buffer (pH 7.4) (Bioenno LifeSciences, CA) or 10% Buffered Formalin Phosphate (Fisher Scientific, ON) for fixation. We tested several fixatives and fixation parameters, such as

470 duration and temperature listed in Table 1. At 21°C, all the fixation, decalcification and washing
471 steps were performed on a low-speed orbital shaker (Corning LSE) set to 55 revolutions per minute
472 (RPM). At 4 °C, all the steps were performed without the low-speed orbital shaker. The *D. magna*
473 samples were immersed in 20X sample volume of fixative. After fixation, samples were washed
474 twice using 1X phosphate-buffered saline (PBS) for 10 min each time. This was followed by
475 decalcification in 20X sample volume of pre-chilled 6% formic acid (Sigma-Aldrich, MO) for 24
476 hours. Samples were then rinsed in 70% ethanol for one minute and immersed in fresh 70% ethanol
477 for 30 min before agarose pre-embedding.
478
479 Table 1: Fixation parameters

Fixative	Fixation time and temperature	Decalcification by cold 6% formic acid time and temperature
Bouin's solution	24 h, 21°C	24 h, 21°C
	48 h, 4°C	24 h, 4°C
	48 h, 21°C	24 h, 21°C
4% Paraformaldehyde	24 h, 21°C	24 h, 21°C
	48 h, 4°C	24 h, 4°C
	48 h, 21°C	24 h, 4°C
10% Buffered Formalin Phosphate	24 h, 4°C	24 h, 21°C
	48 h, 4°C	24 h, 4°C
	48 h, 21°C	24 h, 4°C

480

481 **Mold and agarose embedding**

482 Samples were pre-embedded in 1 % agarose block cast using "triangle mold" (Figure 1A-B) for
483 histological processing following a protocol adapted from Sabaliauskas et al. (2006) (63). After
484 taping around the triangle mold, 2.5 mL of 1 % agarose (Sigma-Aldrich, MO) at 55 °C was pipetted
485 onto the mold, and then allowed to solidify at room temperature (Figure 1C) and, the agarose block
486 was removed gently from the mold (Figure 1D). Then, fixed *D. magna* samples were transferred
487 onto the agarose block using a plastic transfer pipette. A small volume of 70 % ethanol was pipetted
488 onto the block to help with the positioning of samples. Samples designated for the sagittal plane
489 were laid on their sides with a swimming antenna in the wells and all rostra facing the same
490 direction. Samples designated for coronal and transverse orientation were laid on their back in the
491 wells (Figure 1 E-F). Once all the samples were positioned in individual wells, excess ethanol was

492 carefully dried off using lint-free Kimwipes without agitating the samples. Each sample was first
493 topped-off with one drop of molten 1 % agarose (about 50 °C) without moving the sample,
494 followed by a thin layer of 1% agarose covering all the samples. After the agarose solidified (about
495 5 minutes at room temperature), the block was trimmed as needed, placed into a tissue cassette,
496 and stored in 70 % ethanol for tissue processing. During paraffin embedding, the agarose blocks
497 were positioned in the appropriate final orientation (transverse, sagittal or coronal) for sectioning.
498

499 Processing, sectioning, and staining

500 All samples were dehydrated and infiltrated with Formula R paraffin (Leica Biosystems
501 #3801450) in RMC Model 1530 automated closed reagent type tissue processor (Table 2). The *D.*
502 *magna* samples were serially sectioned at 5 µm on a Leica RM2255 automated rotary microtome.
503 Sections were then stained with Harris' hematoxylin and eosin (H&E) in an auto-stainer (Sakura
504 Tissue Tek DRS 2000, IMEB, CA) following a protocol adapted from Copper et al. (2018) (15).
505 The duration of hematoxylin staining was extended from 3 to 7 min to achieve better contrast for
506 samples fixed with Bouin's solution (Table 3). Cover glass No. 1 (Platinum Line) were used for
507 cover-slipping. The use of lower quality cover slips that have inconsistent thicknesses and optical
508 transparency that do not fall within the specifications of the high numerical aperture (n.a.)
509 microscope lenses in most digital scanners, will result in blurred scanned histology images.
510

511 Table 2: Tissue Processing Steps

Duration	Solution	Temp (°C)	Vacuum (in. Hg)
45 min	80% Ethanol	25	15
45 min	95% Ethanol	25	15
1 hour	95% Ethanol	25	15
1 hour (repeat thrice)	100% Ethanol	25	15
1 hour (repeat twice)	Xylene	25	15
1 hour 30 min (repeat twice)	Paraffin	60	15
2 hours	Paraffin	60	15

512
513
514
515

516 Table 3: Automated staining steps

Time	Solution
3 min	Xylene
5 min	Xylene
2 min (repeat twice)	100% Ethanol
2 min	95% Ethanol
10 min	Tap water
7 min	Hematoxylin
1 min	Tap water
1 min	Acidified Alcohol
1 min	Tap water
0.2 min	Ammoniated water
1 min	Tap water
0.3 min	Eosin
1 min	30% Ethanol
1 min	95% Ethanol
1 min	100% Ethanol
1 min	Xylene

517

518 # Histology slide digitization

519 All slides were viewed and screened under microscope using 20X and 40X objective lenses prior
520 to slide imaging. Selected slides were scanned at 40X using an Aperio AT2 slide scanner
521 (LeicaBiosystems, IL) and saved in TIFF format. 40X scanning was performed using 20X
522 objective lens (0.075 n.a. Plan Apo) with 2X optical magnification changer and yields a digital
523 resolution of 0.25-micron per pixel. The regions of selected *D. magna* samples were then extracted
524 using Aperio ImageScope (version 12.4.3.5008). Three channels (Red, Green, Blue) of these
525 digital slides were stacked using Fiji (64) or ImageJ (65), then minimal post-processing was
526 performed in Adobe Photoshop (version 22.1.1). Images were rotated and set to have the same
527 canvas size. The background was removed, the "Exposure" was adjusted (between 0.1 to 0.25 and
528 the same value used for a set of images), and the "Levels" adjusted using preset "Midtones
529 Darker". Each set of digital slides was then pyramidally tiled in preparation for the web-based
530 viewer.

531

532

Labeling and segmentation workflow

For each anatomical structure included in the anatomical ontology, we began by reviewing published literature, then concluding with a visual analysis of the structure in each of the three orthogonally sectioned histology slide sets. Anatomical structures included in the anatomical ontology were grouped and color-coded based on organ systems. Labeling and segmentation of anatomical structures were done one image at a time in Adobe Illustrator (version 25.1). The Adobe Illustrator Layer of an anatomical structure was first labeled corresponding to the appropriate ontological term. Each anatomical structure was segmented by outlining the structure using the curvature tool. Segmentation was then assigned the color based on the ontology. After completion of the labeling and segmentation of all anatomical structures on a given image, a single scalable vector graphic (SVG) was exported to be used as input for the web-based viewer.

Web-interface workflow

The file sizes associated with digital slides are on the order of >2 GB per slide, making scans challenging to view for users with standard computational resources. For easier access and usage of the data without the need to download full-resolution images, we developed an open-access, web-based digital slide viewing platform based on the open-access project OpenSeadragon (https://openseadragon.github.io/). This viewer combines annotations and digital scans into a seamless experience to provide user-friendly access to high-resolution data. The atlas' code was written in client-side JavaScript, HTML, and CSS requires no traditional download and has no server requirement to run the basic implementation. Pyramidally tiled images are parsed and visualized with OpenSeadragon. When the user loads a new image, the viewer opens the corresponding SVG file. The SVG file contains all the anatomical labels on a given image and their corresponding shape vector information. The viewer parses all labels from the SVG file, plotting the corresponding regions on the viewer itself, and updates the ontology to note which regions are available to visualize on the current image.

Acknowledgments

The authors thank Patrick Leibich and the Department of Surgery, Penn State College of Medicine for 3D-SLA printing the casting molds. The authors are grateful to Advanced Light Sources

Beamline 8.3.2, Lawrence Berkeley National Labs for making possible microCT imaging of the *Daphnia* sample. This work was supported by the Penn State Human Health and Environment Seed Grant funded by Pennsylvania Department of Health Commonwealth Universal Research Enhancement Program Grant (to KCA) and the National Institutes of Health (grant 1R24OD18559 to KCC), the Jake Gittlen Laboratories for Cancer Research. The Department of Health specifically disclaims responsibility for any analyses, interpretations, or conclusions. This work contributes to the PrecisionTox project (https://precisiontox.org/) that has received funding from the European Union's Horizon 2020 research and innovation program under grant agreement No 965406.

Competing Interests

The authors declare no competing interest.

References

1. Ebert D. Daphnia as a versatile model system in ecology and evolution. EvoDevo. 2022 Aug 8;13(1):16.

2. Kikuchi M, Sasaki Y, Wakabayashi M. Screening of organophosphate insecticide pollution in water by using Daphnia magna. Ecotoxicol Environ Saf. 2000 Nov 1;47(3):239–45.

3. Tkaczyk A, Bownik A, Dudka J, Kowal K, Ślaska B. Daphnia magna model in the toxicity assessment of pharmaceuticals: A review. Sci Total Environ. 2021 Apr 1;763:143038.

4. Kühn R, Pattard M, Pernak KD, Winter A. Results of the harmful effects of water pollutants to Daphnia magna in the 21 day reproduction test. Water Res. 1989 Apr 1;23(4):501–10.

5. Environmental Protection Agency. Ecological Effects Test Guidelines OCSPP850.1300: Daphnid chronic toxicity test. 1996.

6. Environmental Protection Agency. Methods for Measuring the Acute Toxicity of Effluents and Receiving Waters to Freshwater and Marine Organisms. 2002.

7. OECD. Test No. 202: Daphnia sp. Acute Immobilisation Test [Internet]. Paris: Organisation for Economic Co-operation and Development; 2004 [cited 2021 Nov 4]. Available from: https://www.oecd-ilibrary.org/environment/test-no-202-daphnia-sp-acute-immobilisation-test_9789264069947-en

8. OECD. Daphnia magna Reproduction Test (OECD TG 211) [Internet]. Paris: OECD; 2018 Sep [cited 2021 Nov 4] p. 253–63. Available from: https://www.oecd-ilibrary.org/environment/revised-guidance-document-150-on-standardised-test-guidelines-

595 for-evaluating-chemicals-for-endocrine-disruption/daphnia-magna-reproduction-test-oecd-
596 tg-211_9789264304741-12-en

597 9. Kim HJ, Koedrith P, Seo YR. Ecotoxicogenomic approaches for understanding molecular
598 mechanisms of environmental chemical toxicity using aquatic invertebrate, Daphnia model
599 organism. Int J Mol Sci. 2015 May 29;16(6):12261–87.

600 10. Shaw JR, Pfrender ME, Eads BD, Klaper R, Callaghan A, Sibly RM, et al. Daphnia as an
601 emerging model for toxicological genomics. In: Hogstrand C, Kille P, editors. Advances in
602 Experimental Biology [Internet]. Elsevier; 2008 [cited 2021 Oct 8]. p. 165–328.
603 (Comparative Toxicogenomics; vol. 2). Available from:
604 https://www.sciencedirect.com/science/article/pii/S1872242308000057

605 11. Cheng KC, Katz SR, Lin AY, Xin X, Ding Y. Whole-organism Cellular Pathology: A Systems
606 Approach to Phenomics. Adv Genet. 2016;95:89–115.

607 12. Kumar V, Abbas AK, Aster JC. Robbins & Cotran Pathologic Basis Of Disease (robbins
608 Pathology) [Internet]. Tenth Edition. Elsevier; 2020 [cited 2022 Mar 28]. 1392 p. Available
609 from: https://basi6direct.com/products/9780323531139

610 13. Treuting PM, Dintzis S, Montine KS, editors. Comparative Anatomy and Histology: A Mouse,
611 Rat, and Human Atlas. 2nd edition. London San Diego Cambridge, MA Kidlington:
612 Academic Press; 2017. 570 p.

613 14. Altun ZF, Herndon LA, Wolkow CA, Crocker C, Lints R, Hall DH. WormAtlas [Internet].
614 2002. Available from: http://wormatlas.org

615 15. Copper JE, Budgeon LR, Foutz CA, van Rossum DB, Vanselow DJ, Hubley MJ, et al.
616 Comparative analysis of fixation and embedding techniques for optimized histological
617 preparation of zebrafish. Comp Biochem Physiol Toxicol Pharmacol CBP. 2018 Jun;208:38–
618 46.

619 16. Armit C, Richardson L, Venkataraman S, Graham L, Burton N, Hill B, et al. eMouseAtlas: An
620 atlas-based resource for understanding mammalian embryogenesis. Dev Biol. 2017 Mar
621 1;423(1):1–11.

622 17. Santana LMBM, Damasceno ÉP, Loureiro S, Soares AMVM, Pousão-Ferreira P, Abessa
623 DMS, et al. An Easy-to-Use Histological Technique for Small Biological Samples of
624 Senegalese Sole Larvae. Appl Sci. 2023 Jan;13(4):2346.

625 18. Martinez K, Cupitt J. VIPS ? a highly tuned image processing software architecture. In 2005
626 [cited 2023 Jan 17]. p. 574–7. Available from: https://eprints.soton.ac.uk/262371/

627 19. Fryer G. Functional morphology and the adaptive radiation of the Daphniidae (Branchiopoda:
628 Anomopoda). Philos Trans R Soc Lond B Biol Sci. 1991 Jan 29;331(1259):1–99.

629 20. Agar WE. The swimming setae of Daphnia carinata. J Cell Sci. 1950 Dec 1;s3-91(16):353–
630 68.

631 21. Auld SKJR, Scholefield JA, Little TJ. Genetic variation in the cellular response of Daphnia
632 magna (Crustacea: Cladocera) to its bacterial parasite. Proc R Soc B Biol Sci. 2010 Nov
633 7;277(1698):3291–7.

634 22. Bednarska A. Adaptive changes in morphology of Daphnia filter appendages in response to
635 food stress. Polish Journal of Ecology. 2006;54:663–8.

636 23. Benzie JAH. The Genus Daphnia (including Daphniopsis) (Anomopoda:Daphniidae). Kenobi
637 Productions; 2005. 388 p.

638 24. Binder G. Das Muskelsystem von Daphnia. Int Rev Gesamten Hydrobiol Hydrogr. 1931;26(1–
639 2):54–98.

640 25. Christensen AK, Owusu NG, Jean-Louis D. Carapace epithelia are rich in large filamentous
641 actin bundles in Daphnia magna, Daphnia pulex, and Sida crystallina (Crustacea: Cladocera).
642 Invertebr Biol. 2018;137(1):49–59.

643 26. Consi TR, Macagno ER, Necles N. The oculomotor system of Daphnia magna. The eye
644 muscles and their motor neurons. Cell Tissue Res. 1987 Mar;247(3):515–23.

645 27. Ebert D. Introduction to Daphnia Biology [Internet]. Ecology, Epidemiology, and Evolution
646 of Parasitism in Daphnia [Internet]. National Center for Biotechnology Information (US);
647 2005 [cited 2021 Mar 14]. Available from: https://www.ncbi.nlm.nih.gov/books/NBK2042/

648 28. Edwards C. The anatomy of Daphnia mandibles. Trans Am Microsc Soc. 1980;99(1):2–24.

649 29. Goldmann T, Becher B, Wiedorn KH, Pirow R, Deutschbein ME, Vollmer E, et al. Epipodite
650 and fat cells as sites of hemoglobin synthesis in the branchiopod crustacean Daphnia magna.
651 Histochem Cell Biol. 1999 Nov;112(5):335–9.

652 30. Halcrow K. The fine structure of the carapace integument of Daphnia magna Straus (Crustacea
653 Branchiopoda). Cell Tissue Res. 1976 Jun 14;169(2):267–76.

654 31. Hiruta C, Tochinai S. Formation and structure of the ephippium (resting egg case) in relation
655 to molting and egg laying in the water flea Daphnia pulex De Geer (Cladocera: Daphniidae).
656 J Morphol. 2014 Jul;275(7):760–7.

657 32. Kikuchi S. The fine structure of the gill epithelium of a fresh-water flea, Daphnia magna
658 (Crustacea: Phyllopoda) and changes associated with acclimation to various salinities. I.
659 Normal fine structure. Cell Tissue Res. 1983;229(2):253–68.

660 33. Kress T, Harzsch S, Dircksen H. Neuroanatomy of the optic ganglia and central brain of the
661 water flea Daphnia magna (Crustacea, Cladocera). Cell Tissue Res. 2016 Mar 1;363(3):649–
662 77.

663 34. McCoole MD, Baer KN, Christie AE. Histaminergic signaling in the central nervous system
664 of Daphnia and a role for it in the control of phototactic behavior. J Exp Biol. 2011 May
665 15;214(Pt 10):1773–82.

666 35. Metschnikoff E. A disease of Daphnia caused by a yeast. A contribution to the theory of
667 phagocytes as agents for attack on disease-causing organisms. Archiv Pathol Anat Physiol
668 Klin Med. 1884;96:177–95.

669 36. Rossi F. Comparative observations on the female reproductive system and parthenogenetic
670 oogenesis in Cladocera. Bolletino Zool. 1980 Jan;47(1–2):21–38.

671 37. Schultz TW, Kennedy JR. The fine structure of the digestive system of Daphnia pulex
672 (Crustacea: Cladocera). Tissue Cell. 1976 Jan 1;8(3):479–90.

673 38. Smirnov NN. Physiology of the Cladocera. Physiol Cladocera. 2013 Oct 1;1–336.

674 39. Stein RJ, Richter WR, Zussman RA, Brynjolfsson G. Ultrastructural characterization of
675 Daphnia heart muscle. J Cell Biol. 1966 Apr 1;29(1):168–70.

676 40. Steinsland AJ. Heart ultrastructure in Daphnia pulex De Geer (Crustacea, Branchiopoda,
677 Cladocera). J Crustac Biol. 1982;2(1):54–8.

678 41. Quaglia A, Sabelli B, Villani L. Studies on the intestine of Daphnidae (Crustacea, Cladocera)
679 ultrastructure of the midgut of Daphnia magna and Daphnia obtusa. J Morphol.
680 1976;150(3):711–25.

681 42. Weiss LC, Tollrian R, Herbert Z, Laforsch C. Morphology of the Daphnia nervous system: a
682 comparative study on Daphnia pulex, Daphnia lumholtzi, and Daphnia longicephala. J
683 Morphol. 2012 Dec;273(12):1392–405.

684 43. Wuerz M, Huebner E, Huebner J. The morphology of the male reproductive system,
685 spermatogenesis and the spermatozoon of Daphnia magna (Crustacea: Branchiopoda). J
686 Morphol. 2017 Nov;278(11):1536–50.

687 44. Zaffagnini F, Zeni C. Considerations on some cytological and ultrastructural observations on
688 fat cells of Daphnia (Crustacea, Cladocera). Bollettino di zoologia. 1986;53(1):33–9.

689 45. Zaffagnini F, Zeni C. Ultrastructural investigations on the labral glands of Daphnia obtusa
690 (Crustacea, Cladocera). J Morphol. 1987 Jul;193(1):23–33.

691 46. Zeni C, Franchini A. A preliminary histochemical study on the labral glands of Daphnia obtusa
692 (Crustacea, Cladocera). Acta Histochem. 1990;88:175–81.

693 47. Decaestecker E, De Meester L, Mergeay J. Cyclical parthenogenesis in Daphnia: sexual versus
694 asexual reproduction. In: Schön I, Martens K, Dijk P, editors. Lost Sex: The Evolutionary
695 Biology of Parthenogenesis [Internet]. Dordrecht: Springer Netherlands; 2009 [cited 2022
696 Jan 21]. p. 295–316. Available from: https://doi.org/10.1007/978-90-481-2770-2_15

697 48. Chen L, Barnett RE, Horstmann M, Bamberger V, Heberle L, Krebs N, et al. Mitotic activity
698 patterns and cytoskeletal changes throughout the progression of diapause developmental
699 program in Daphnia. BMC Cell Biol. 2018 Dec 29;19:30.

700 49. Cáceres CE. Interspecific variation in the abundance, production, and emergence of Daphnia
701 diapausing eggs. Ecology. 1998;79(5):1699–710.

702 50. Mergeay J, Verschuren D, Kerckhoven LV, Meester LD. Two hundred years of a diverse
703 Daphnia community in Lake Naivasha (Kenya): effects of natural and human-induced
704 environmental changes. Freshw Biol. 2004;49(8):998–1013.

705 51. Beaton MJ, Hebert PDN. Miniature genomes and endopolyploidy in cladoceran crustaceans.
706 Genome. 1989 Dec 1;32(6):1048–53.

707 52. Bodar CWM, van Donselaar EG, Herwig HJ. Cytopathological investigations of digestive tract
708 and storage cells in Daphnia magna exposed to cadmium and tributyltin. Aquat Toxicol. 1990
709 Oct 1;17(4):325–37.

710 53. Yang XY, Edelmann RE, Oris JT. Suspended C60 nanoparticles protect against short-term UV
711 and fluoranthene photo-induced toxicity, but cause long-term cellular damage in Daphnia
712 magna. Aquat Toxicol. 2010 Oct 15;100(2):202–10.

713 54. Heinlaan M, Kahru A, Kasemets K, Arbeille B, Prensier G, Dubourguier HC. Changes in the
714 Daphnia magna midgut upon ingestion of copper oxide nanoparticles: A transmission
715 electron microscopy study. Water Res. 2011 Jan 1;45(1):179–90.

716 55. Bacchetta R, Santo N, Marelli M, Nosengo G, Tremolada P. Chronic toxicity effects of ZnSO4
717 and ZnO nanoparticles in Daphnia magna. Environ Res. 2017 Jan 1;152:128–40.

718 56. Castejón D, Alba-Tercedor J, Rotllant G, Ribes E, Durfort M, Guerao G. Micro-computed
719 tomography and histology to explore internal morphology in decapod larvae. Sci Rep. 2018
720 Sep 26;8(1):14399.

721 57. Schulz G, Waschkies C, Pfeiffer F, Zanette I, Weitkamp T, David C, et al. Multimodal imaging
722 of human cerebellum - merging X-ray phase microtomography, magnetic resonance
723 microscopy and histology. Sci Rep. 2012 Nov 9;2(1):826.

724 58. Connelly SJ, Walling K, Wilbert SA, Catlin DM, Monaghan CE, Hlynchuk S, et al. UV-
725 Stressed Daphnia pulex increase fitness through uptake of Vitamin D3. PLOS ONE. 2015 Jul
726 6;10(7):e0131847.

727 59. Mittmann B, Ungerer P, Klann M, Stollewerk A, Wolff C. Development and staging of the
728 water flea Daphnia magna (Straus, 1820; Cladocera, Daphniidae) based on morphological
729 landmarks. EvoDevo. 2014 Mar 18;5(1):12.

730 60. Ding Y, Vanselow DJ, Yakovlev MA, Katz SR, Lin AY, Clark DP, et al. Computational 3D
731 histological phenotyping of whole zebrafish by X-ray histotomography. White RM, Stainier
732 DY, Ekker SC, editors. eLife. 2019 May 7;8:e44898.

733 61. Yakovlev MA, Vanselow DJ, Ngu MS, Zaino CR, Katz SR, Ding Y, et al. A wide-field micro-
734 computed tomography detector: micron resolution at half-centimetre scale. J Synchrotron

735 Radiat [Internet]. 2022 Mar 1 [cited 2022 Feb 22];29(2). Available from:
736 https://journals.iucr.org/s/issues/2022/02/00/mo5248/

737 62. Cheng KC, Burdine RD, Dickinson ME, Ekker SC, Lin AY, Lloyd KCK, et al. Promoting
738 validation and cross-phylogenetic integration in model organism research. Dis Model Mech.
739 2022 Sep 20;15(9):dmm049600.

740 63. Sabaliauskas NA, Foutz CA, Mest JR, Budgeon LR, Sidor AT, Gershenson JA, et al. High-
741 throughput zebrafish histology. Methods. 2006 Jul 1;39(3):246–54.

742 64. Schindelin J, Arganda-Carreras I, Frise E, Kaynig V, Longair M, Pietzsch T, et al. Fiji: an
743 open-source platform for biological-image analysis. Nat Methods. 2012 Jul;9(7):676–82.

744 65. Schneider CA, Rasband WS, Eliceiri KW. NIH Image to ImageJ: 25 years of image analysis.
745 Nat Methods. 2012 Jul;9(7):671–5.

746 66. Haney JF, Hall DJ. Sugar-coated Daphnia: A preservation technique for Cladocera1. Limnol
747 Oceanogr. 1973;18(2):331–3.

748

Supporting information

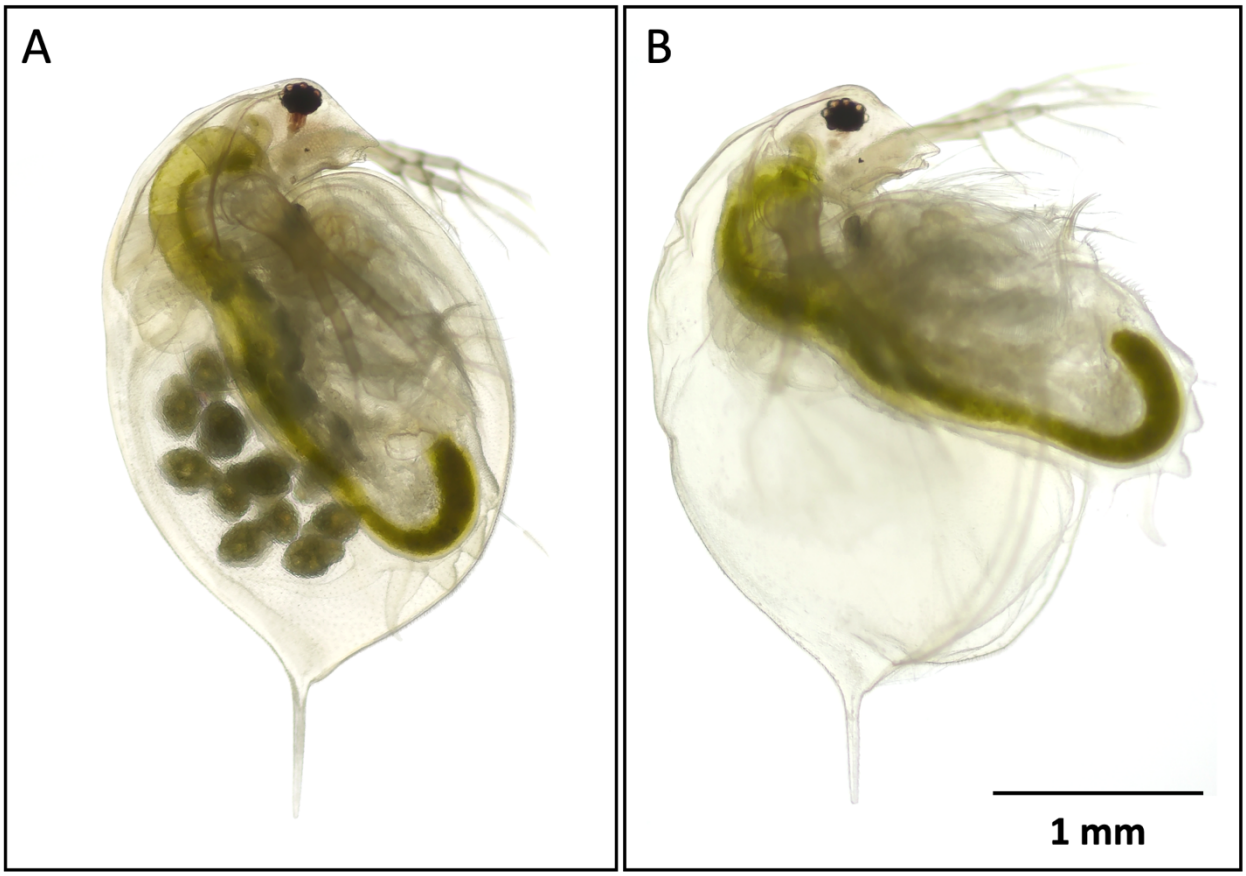

S1 Figure. "Ballooning" artifact observed in *D. magna* sample fixed with 4% PFA and 10% NBF. (A) A well-preserved *D. magna* sample. (B) A *D. magna* sample with the "ballooning" artifact. This artifact is characterized by bulging of the carapace and ventral extension of the postabdomen. When both occurred, eggs or embryos were released from the brood chambers. Ballooned samples were difficult to orient during agarose pre-embedding. The mechanism of ballooning is unclear. Haney and Hall (1973) (66) suggested that it is likely related to a death-induced osmotic imbalance of the connective tissue that attached the carapace to the animal's body. Fixation at 4 °C prevented this artifact, but it recurred after de-calcification in cold 6% formic acid at 4° C.

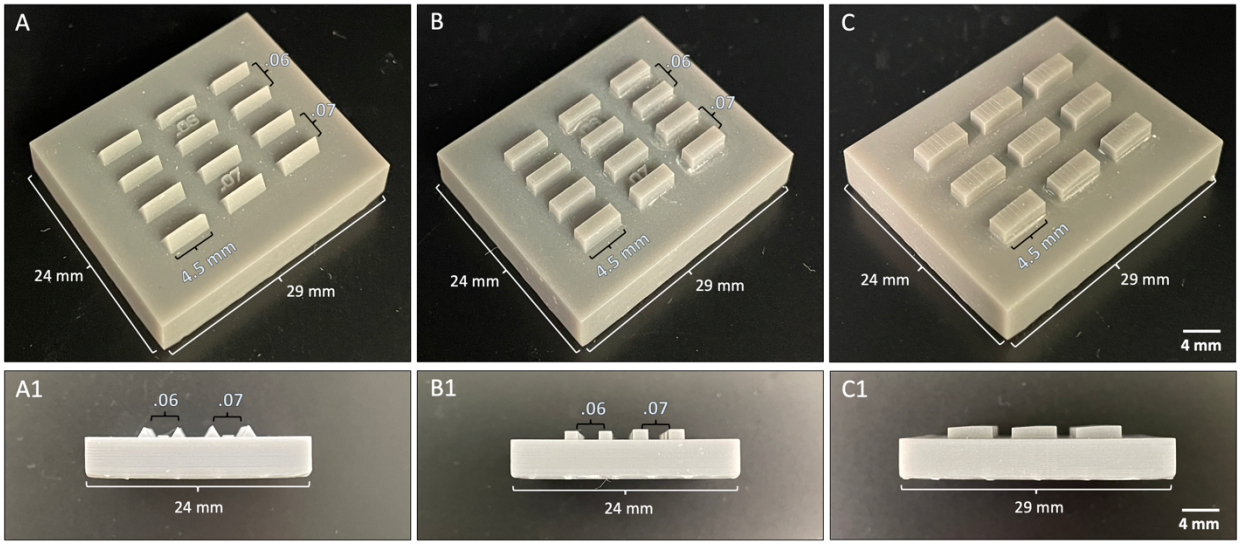

S3 Figure. 3D-SLA printed casting molds of different teeth designs that were tested for orientation and positioning of *Daphnia* samples. (A) Top and **(A1)** side view of the mold with triangular teeth height and the widest width of 1.5 mm (indicated by .06) and 1.8 mm (indicated by .07). **(B)** Top and **(B1)** side view of the mold with rectangular teeth height and width of 1.5 mm (indicated by .06) and 1.8 mm (indicated by .07). **(C)** Top and **(C1)** side view of the mold with sloped rectangular teeth. We learned from embedding trials that the rectangular and sloped rectangular molds are not versatile for *Daphnia* samples and are challenging to hold samples in place either laying on their side or back. Triangular mold with teeth length of 4.5 mm, and height and width of 1.5 mm allowed precise positioning of *D. magna* samples with ease.